Global fit to Higgs signal strengths and couplings and implications for extended Higgs sectors

G. Bélanger,[1,*] B. Dumont,[2,†] U. Ellwanger,[3,‡] J. F. Gunion,[4,§] and S. Kraml[2,‖]

[1]*LAPTH, Université de Savoie, CNRS, B.P. 110, F-74941 Annecy-le-Vieux Cedex, France*

[2]*Laboratoire de Physique Subatomique et de Cosmologie, UJF Grenoble 1, CNRS/IN2P3, INPG, 53 Avenue des Martyrs, F-38026 Grenoble, France*

[3]*Laboratoire de Physique Théorique, UMR 8627, CNRS and Université de Paris–Sud, F-91405 Orsay, France*

[4]*Department of Physics, University of California, Davis, California 95616, USA*

(Received 22 July 2013; published 15 October 2013)

The most recent LHC data have provided a considerable improvement in the precision with which various Higgs production and decay channels have been measured. Using all available public results from ATLAS, CMS and the Tevatron, we derive for each final state the combined confidence level contours for the signal strengths in the (gluon fusion + top-quark pair associated production) versus (vector boson fusion + associated production with vector bosons) space. These ''combined signal strength ellipses'' can be used in a simple, generic way to constrain a very wide class of new physics models in which the couplings of the Higgs boson deviate from the Standard Model prediction. Here, we use them to constrain the reduced couplings of the Higgs boson to up-quarks, down-quarks/leptons and vector boson pairs. We also consider new physics contributions to the loop-induced gluon-gluon and photon-photon couplings of the Higgs, as well as invisible/unseen decays. Finally, we apply our fits to some simple models with an extended Higgs sector, in particular to two-Higgs-doublet models of Type I and Type II, the inert doublet model, and the Georgi-Machacek triplet Higgs model.

DOI: 10.1103/PhysRevD.88.075008 PACS numbers: 12.60.Fr, 14.80.Bn, 14.80.Ec, 12.60.−i

I. INTRODUCTION

That the mass of the Higgs boson is about 125–126 GeV is a very fortunate circumstance in that we can detect it in many different production and decay channels [1,2]. Indeed, many distinct signal strengths, defined as production × decay rates relative to Standard Model (SM) expectations, $\mu_i \equiv (\sigma \times \mathrm{BR})_i/(\sigma \times \mathrm{BR})_i^{\mathrm{SM}}$, have been measured with unforeseeable precision already with the 7–8 TeV LHC run [3,4]. From these signal strengths one can obtain information about the couplings of the Higgs boson to electroweak gauge bosons, fermions (of the third generation) and loop-induced couplings to photons and gluons.

According to the latest measurements presented at the 2013 Moriond [3–17] and LHCP [18–20] conferences, these couplings seem to coincide well with those expected in the SM. This poses constraints on various beyond the Standard Model (BSM) theories, in which these couplings can differ substantially from those of the SM. The Higgs couplings can be parametrized in terms of effective Lagrangians [21–57] whose structure depends, however, on the class of models considered, such as extended Higgs sectors, extra fermions and/or scalars contributing to loop diagrams, composite Higgs bosons and/or fermions, nonlinear realizations of electroweak symmetry breaking, large extra dimensions, Higgs-dilaton mixing and more.

When such generalized couplings are used to fit the large number of measurements of signal strengths now available in different channels, one faces the problem that the experimentally defined signal categories (based on combinations of cuts) nearly always contain superpositions of different production modes and thus errors (both systematic and statistical) in different channels are correlated. Ideally one would like to fit not to experimentally defined categories but rather to the different production and decay modes that lead to distinct final states and kinematic distributions. The five usual theoretically ''pure'' production modes are gluon-gluon fusion (ggF), vector boson fusion (VBF), associated production with a W or Z boson (WH and ZH, commonly denoted as VH), and associated production with a top-quark pair (ttH). The scheme conveniently adopted by the experimental collaborations is to group these five modes into just two effective modes ggF + ttH and VBF + VH and present contours of constant likelihood $\mathcal{L}$ for particular final states in the μ(ggF + ttH) versus μ(VBF + VH) plane. This is a natural choice for the following reasons:

(i) Deviations from custodial symmetry, which implies a SM-like ratio of the couplings to W and Z gauge bosons, are strongly constrained by the Peskin-Takeuchi T parameter [58,59] from electroweak fits [60]. Furthermore, there is no indication of such deviation from the Higgs measurements performed at the LHC [3,4]. Hence, one can assume that the VBF and VH production modes both depend on a

*belanger@lapth.cnrs.fr
†dumont@lpsc.in2p3.fr
‡Ulrich.Ellwanger@th.u-psud.fr
§jfgunion@ucdavis.edu
‖sabine.kraml@lpsc.in2p3.fr

single generalized coupling of the Higgs boson to $V = W, Z$ and it is therefore appropriate to combine results for these two channels.

(ii) Grouping ggF and ttH together is more a matter of convenience in order to be able to present two-dimensional likelihood plots. Nonetheless, there are some physics motivations for considering this combination, the primary one being that, in the current data set, ggF and ttH are statistically independent since they are probed by different final states: ttH via $H \to b\bar{b}$ and ggF via a variety of other final states such as $\gamma\gamma$ and ZZ^*. While the ttH production rate depends entirely on the $Ht\bar{t}$ coupling, ggF production occurs at one loop and is sensitive to both the $Ht\bar{t}$ coupling and the $Hb\bar{b}$ couplings as well as to BSM loop diagrams. Although in the SM limit ggF is roughly 90% determined by the $Ht\bar{t}$ coupling, leading to a strong correlation with the ttH process, this need not be the case in models with suppressed $Ht\bar{t}$ coupling and/or enhanced $Hb\bar{b}$ coupling and most especially in models with BSM loops.

The final states in which the Higgs is observed include $\gamma\gamma$, $ZZ^{(*)}$, $WW^{(*)}$, $b\bar{b}$ and $\tau\tau$. However, they do not all scale independently. In particular, custodial symmetry implies that the branching fractions into $ZZ^{(*)}$ and $WW^{(*)}$ are rescaled by the same factor with respect to the SM. We are then left with two independent production modes (VBF + VH) and (ggF + ttH), and four independent final states $\gamma\gamma$, $VV^{(*)}$, $b\bar{b}$, $\tau\tau$. In addition, in many models there is a common coupling to down-type fermions, and hence the branching fractions into $b\bar{b}$ and $\tau\tau$ rescale by a common factor, leading to identical μ values for the $b\bar{b}$ and $\tau\tau$ final states.

The first purpose of the present paper is to combine the information provided by ATLAS, CMS and the Tevatron experiments on the $\gamma\gamma$, $ZZ^{(*)}$, $WW^{(*)}$, $b\bar{b}$ and $\tau\tau$ final states including the error correlations among the (VBF + VH) and (ggF + ttH) production modes. Using a Gaussian approximation, we derive for each final state a combined likelihood in the $\mu(\text{ggF} + \text{ttH})$ versus $\mu(\text{VBF} + \text{VH})$ plane, which can then simply be expressed as a χ^2. (Note that this does *not* rely on ggF production being dominated by the top loop.) We express this χ^2 as

$$\chi_i^2 = a_i(\mu_i^{\text{ggF}} - \hat{\mu}_i^{\text{ggF}})^2 + 2b_i(\mu_i^{\text{ggF}} - \hat{\mu}_i^{\text{ggF}}) \times (\mu_i^{\text{VBF}} - \hat{\mu}_i^{\text{VBF}}) + c_i(\mu_i^{\text{VBF}} - \hat{\mu}_i^{\text{VBF}})^2, \quad (1)$$

where the upper indices ggF and VBF stand for (ggF + ttH) and (VBF + VH), respectively, the lower index i stands for $\gamma\gamma$, $VV^{(*)}$, $b\bar{b}$ and $\tau\tau$ (or $b\bar{b} = \tau\tau$), and $\hat{\mu}_i^{\text{ggF}}$ and $\hat{\mu}_i^{\text{VBF}}$ denote the best-fit points obtained from the measurements. We thus obtain "combined likelihood ellipses," which can be used in a simple, generic way to constrain nonstandard Higgs sectors and new contributions to the loop-induced processes, provided they have the same Lagrangian structure as the SM.

In particular, these likelihoods can be used to derive constraints on a model-dependent choice of generalized Higgs couplings, the implications of which we study subsequently for several well-motivated models. The choice of models is far from exhaustive, but we present our results for the likelihoods as a function of the independent signal strengths μ_i in such a manner that these can easily be applied to other models.

We note that we will not include correlations between different final states but identical production modes that originate from common theoretical errors on the production cross sections [51,57] nor correlations between systematic errors due to common detector components (like electromagnetic calorimeters) sensitive to different final states (such as $\gamma\gamma$ and e^- from $ZZ^{(*)}$ and $WW^{(*)}$). A precise treatment of these "second order" corrections to our contours is possible only if performed by the experimental collaborations. It is, however, possible to estimate their importance, e.g., by reproducing the results of coupling fits performed by ATLAS and CMS, as done for two representative cases in Appendix B. The results we obtain are in good agreement with the ones published by the experimental collaborations.

In the next section, we will list the various sources of information used for the determination of the coefficients a_i, b_i, c_i, $\hat{\mu}_i^{\text{ggF}}$ and $\hat{\mu}_i^{\text{VBF}}$, and present our results for these parameters. In Sec. III, we parametrize the signal strengths μ_i in terms of various sets of Higgs couplings, and use our results from Sec. II to derive χ^2 contours for these couplings. In Sec. IV, we apply our fits to some concrete BSM models, which provide simple tree-level relations between the generalized Higgs couplings to fermions and gauge bosons. Our conclusions are presented in Sec. V. The Appendix contains clarifying details on Eq. (1) as well as a comparison with coupling fits performed by ATLAS and CMS.

II. TREATMENT OF THE EXPERIMENTAL RESULTS AND COMBINED SIGNAL STRENGTH ELLIPSES

The aim of the present section is to combine the most recent available information on signal strengths from the ATLAS, CMS and Tevatron experiments for the various Higgs decay modes. In most cases, these include error correlations in the plane of the (VBF + VH) and (ggF + ttH) production modes. For practical purposes it is very useful to represent the likelihoods in these planes in the Gaussian approximation. Once the expressions for the various χ_i^2 are given in the form of Eq. (1), it becomes straightforward to evaluate the numerical value of $\chi^2 = \sum_i \chi_i^2$ in any theoretical model with a SM-like Lagrangian structure, in which predictions for the Higgs branching

TABLE I. Combined best-fit signal strengths $\hat{\mu}^{\rm ggF}$, $\hat{\mu}^{\rm VBF}$ and correlation coefficient ρ for various final states, as well as the coefficients a, b and c for the χ^2 in Eq. (1).

	$\hat{\mu}^{\rm ggF}$	$\hat{\mu}^{\rm VBF}$	ρ	a	b	c
$\gamma\gamma$	0.98 ± 0.28	1.72 ± 0.59	-0.38	14.94	2.69	3.34
VV	0.91 ± 0.16	1.01 ± 0.49	-0.30	44.59	4.24	4.58
$b\bar{b}/\tau\tau$	0.98 ± 0.63	0.97 ± 0.32	-0.25	2.67	1.31	10.12
$b\bar{b}$	-0.23 ± 2.86	0.97 ± 0.38	0	0.12	0	7.06
$\tau\tau$	1.07 ± 0.71	0.94 ± 0.65	-0.47	2.55	1.31	3.07

fractions and the (VBF + VH) and (ggF + ttH) production modes (relative to the SM) can be made.

From the corresponding information provided by the experimental collaborations one finds that the Gaussian approximation is justified in the neighborhood [68% confidence level (C.L.) contours] of the best-fit points. Hence we parametrize these 68% C.L. contours, separately for each experiment, as in Eq. (1).[1] Occasionally, only a single signal rate including error bars for a specific final state is given. Using the relative contributions from the various production modes, this kind of information can still be represented in the form of Eq. (1), leading to an "ellipse" that reduces to a strip in the plane of the (VBF + VH) and (ggF + ttH) production modes.

Subsequently these expressions can easily be combined and be represented again in the form of Eq. (1). We expect that the result is reliable up to $\chi^2_i \lesssim 6$ (making it possible to derive 95% C.L. contours), but its extrapolation to (much) larger values of χ^2_i should be handled with care.

Starting with the $H \to \gamma\gamma$ final state, we treat in this way the 68% C.L. contours given by ATLAS in [4,6,8], by CMS in [3,11,20][2] and the Tevatron in [18]. [In the case of the Tevatron, for all final states only a strip in the plane of the (VBF + VH) and (ggF + ttH) production modes is defined.] For the combination of the ZZ and WW final states, we use the 68% C.L. contours given by ATLAS for ZZ in [4,7,8], by CMS for ZZ in [3,12], by ATLAS for WW in [4,9], by CMS for WW in [3,13,15] and by the Tevatron for WW in [18]. For the combination of the $b\bar{b}$ and $\tau\tau$ final states, we use the "strip" defined by the ATLAS result for $b\bar{b}$ in associated VH production from [62], the 68% C.L. contour given by CMS for $b\bar{b}$ in [19], the Tevatron result for $b\bar{b}$ from [18] and combine them with the ATLAS 68% C.L. contour for $\tau\tau$ from [4,63] and the CMS 68% C.L. contours for $\tau\tau$ from [3,14]. We also use the ATLAS search for $ZH \to \ell^+\ell^- +$ invisible, extracting the likelihood from Fig. 10(b) of [5]. All the above 68% C.L. likelihood contours are parametrized by ellipses (or strips) in χ^2 as in Eq. (1), which can subsequently be combined. (In Appendix A we clarify how these combinations are performed.)

The resulting parameters $\hat{\mu}^{\rm ggF}$, $\hat{\mu}^{\rm VBF}$, a, b and c for Eq. (1) (and, for completeness, the correlation coefficient ρ) for the different final states are listed in Table I. The corresponding 68%, 95% and 99.7% C.L. ellipses are represented graphically in Fig. 1.

We see that, after combining different experiments, the best-fit signal strengths are astonishingly close to their SM values, the only exception being the $\gamma\gamma$ final state produced via (VBF + VH) for which the SM is, nonetheless, still within the 68% C.L. contour. Therefore, these results serve mainly to constrain BSM contributions to the properties of the Higgs boson.

The combination of the $b\bar{b}$ and $\tau\tau$ final states is justified, in principle, in models where one specific Higgs doublet has the same reduced couplings (with respect to the SM) to down-type quarks and leptons. However, even in this case QCD corrections and so-called Δ_b corrections (from radiative corrections, notably at large $\tan\beta$, inducing couplings of another Higgs doublet to b quarks; see e.g. [64,65]) can lead to deviations of the reduced Hbb and $H\tau\tau$ couplings from a common value. Therefore, for completeness we show the result for the $b\bar{b}$ final state only (combining ATLAS, CMS and Tevatron results as given in the previous paragraph) in the fourth line of Table I, and the resulting 68%, 95% and 99.7% C.L. contours in the left plot of Fig. 2. The result for the $\tau\tau$ final state only (combining ATLAS and CMS results as given in the previous paragraph) is shown in the fifth line of Table I, and the resulting 68%, 95% and 99.7% C.L. contours in the right plot in Fig. 2.

Before proceeding, a comment is in order regarding the impact of the Tevatron results. While for the $\gamma\gamma$ and VV final states, our combined likelihoods are completely dominated by the LHC measurements, to the extent that they are the same with or without including the Tevatron results, this is not the case for the $b\bar{b}$ final state. For illustration, in the plots for the $b\bar{b}$ final state in Figs. 1 and 2 we also show what would be the result neglecting the Tevatron measurements.

III. FITS TO REDUCED HIGGS COUPLINGS

Using the results of the previous section, it is straightforward to determine constraints on the couplings of the observed Higgs boson to various particle pairs, assuming only a SM-like Lagrangian structure. As in [45], we define C_U, C_D and C_V to be ratios of the H coupling to up-type

[1] This corresponds to fitting a bivariate normal distribution to the 68% C.L. contours. We have verified that this reproduces sufficiently well the best-fit points as well as the 95% C.L. contours; see Sec. 2 of Ref. [61] for more detail.

[2] Note that we are using the multivariate analysis for CMS $H \to \gamma\gamma$. The cut-based analysis (CiC) also presented by CMS [10]—that leads to higher but compatible signal strengths—is unfortunately not available in the form of contours in the plane of the (VBF + VH) and (ggF + ttH) production modes. Moreover, no information is given on the subchannel decomposition, so in fact the CMS CiC analysis cannot be used for our purpose.

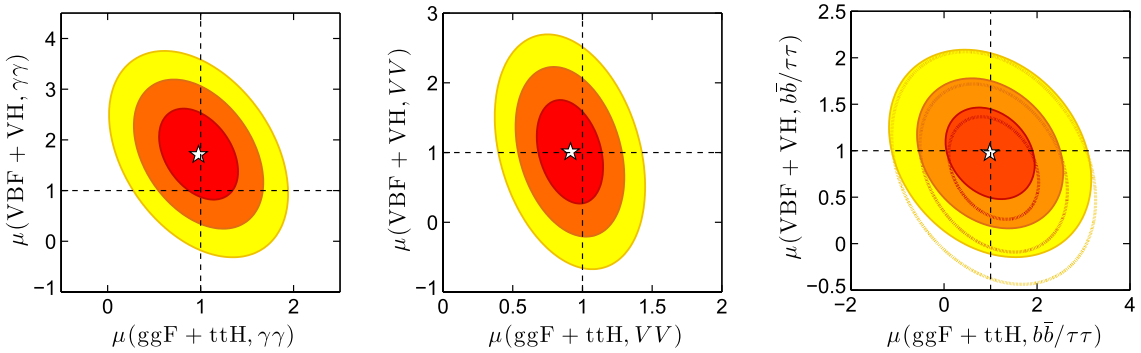

FIG. 1 (color online). Combined signal strength ellipses for the $\gamma\gamma$, $VV = ZZ$, WW and $b\bar{b} = \tau\tau$ channels. The filled red, orange and yellow ellipses show the 68%, 95% and 99.7% C.L. regions, respectively, derived by combining the ATLAS, CMS and Tevatron results. The red, orange and yellow line contours in the rightmost plot show how these ellipses change when neglecting the Tevatron results. The white stars mark the best-fit points.

quarks, down-type quarks and leptons, and vector boson pairs, respectively, relative to that predicted in the case of the SM Higgs boson (with $C_V > 0$ by convention). In addition to these tree-level couplings there are also the one-loop induced couplings of the H to gg and $\gamma\gamma$. Given values for C_U, C_D and C_V the contributions of SM particles to the gg and $\gamma\gamma$ couplings, denoted $\bar{C}_g$ and $\bar{C}_\gamma$, respectively, can be computed. We take into account next-to-leading order corrections to $\bar{C}_g$ and $\bar{C}_\gamma$ as recommended by the LHC Higgs Cross Section Working Group [66]. In particular we include all the available QCD corrections for C_g using HIGLU [67,68] and for C_γ using HDECAY [68,69], and we switch off the electroweak corrections. In some of the fits below, we will also allow for additional new physics contributions to C_g and C_γ by writing $C_g = \bar{C}_g + \Delta C_g$ and $C_\gamma = \bar{C}_\gamma + \Delta C_\gamma$.

We note that in presenting one- (1D) and two-dimensional (2D) distributions of $\Delta\chi^2$, those quantities among C_U, C_D, C_V, ΔC_g and ΔC_γ not plotted, but that are treated as variables, are being profiled over. The fits presented below will be performed with and without allowing for invisible decays of the Higgs boson. In the latter case, only SM decay modes are present. In the former case, the new decay modes are assumed to produce invisible or undetected particles that would be detected as missing transverse energy at the LHC. A direct search for invisible decays of the Higgs boson have been performed by ATLAS in the $ZH \to \ell^+\ell^- + E_T^{\mathrm{miss}}$ channel [5] and is implemented in the analysis. Thus, the total width is fully calculable from the set of C_i and $\mathcal{B}(H \to \text{invisible})$ in all the cases we consider. (We will come back to this at the end of this section.)

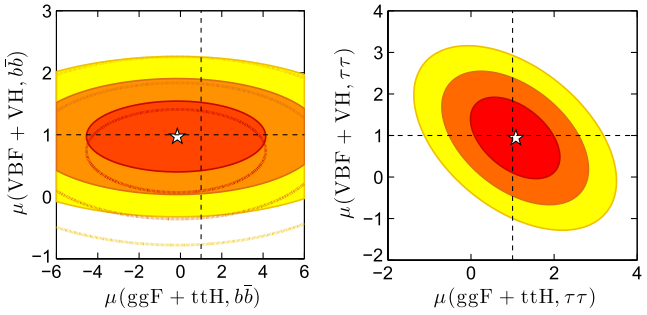

FIG. 2 (color online). Combined signal strength ellipses as in Fig. 1 but treating the couplings to $b\bar{b}$ and $\tau\tau$ separately.

We begin by taking SM values for the tree-level couplings to fermions and vector bosons, i.e. $C_U = C_D = C_V = 1$, but allow for new physics contributions to the couplings to gg and $\gamma\gamma$. The fit results with and without allowing for invisible/unseen Higgs decays are shown in Fig. 3. We observe that the SM point of $\Delta C_g = \Delta C_\gamma = 0$ is well within the 68% contour with the best-fit points favoring a slightly positive (negative) value for ΔC_γ (ΔC_g). Allowing for invisible/unseen decays expands the 68%, 95% and 99.7% C.L. regions by only a modest amount. This is in contrast to the situation at the end of 2012 [45,48], where some new physics contribution to both ΔC_g and ΔC_γ was preferred, and allowing for invisible decays had a large effect; with the higher statistics and with the reduced $\gamma\gamma$ signal strength from CMS [11], ΔC_g and ΔC_γ are now much more constrained. The best fit is obtained for $\Delta C_g = -0.06$, $\Delta C_\gamma = 0.13$, $\mathcal{B}_{\mathrm{inv}} \equiv \mathcal{B}(H \to \text{invisible}) = 0$ and has $\chi^2_{\mathrm{min}} = 17.71$ for 21 degrees of freedom (d.o.f.),[3] as compared to $\chi^2 = 18.95$ with 23 d.o.f. for the SM, so allowing for additional loop contributions does not improve the fit.

Next, we allow C_U, C_D and C_V to vary but assume that there is no new physics in the gg and $\gamma\gamma$ loops; i.e. we take $\Delta C_g = \Delta C_\gamma = 0$. Results for this case are shown in Fig. 4. We observe that, contrary to the situation at the end of 2012 [45], the latest data prefer a positive value of C_U close to 1. This is good news, as a negative sign of C_U—in the

[3]There are in total 23 measurements entering our fit, and we adopt the simple definition of the number of d.o.f. as the number of measurements minus the number of parameters.

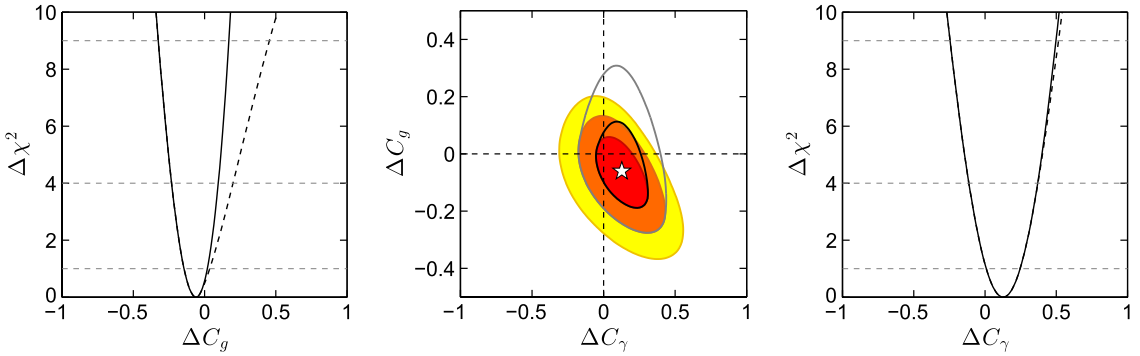

FIG. 3 (color online). $\Delta\chi^2$ distributions in 1D and 2D for the fit of ΔC_g and ΔC_γ for $C_U = C_D = C_V = 1$. In the 1D plots, the solid (dashed) lines are for the case that invisible/unseen decays are absent (allowed). In the 2D plot, the red, orange and yellow areas are the 68%, 95% and 99.7% C.L. regions, respectively, assuming invisible decays are absent. The white star marks the best-fit point. The black and grey lines show the 68% and 95% C.L. contours when allowing for invisible decays.

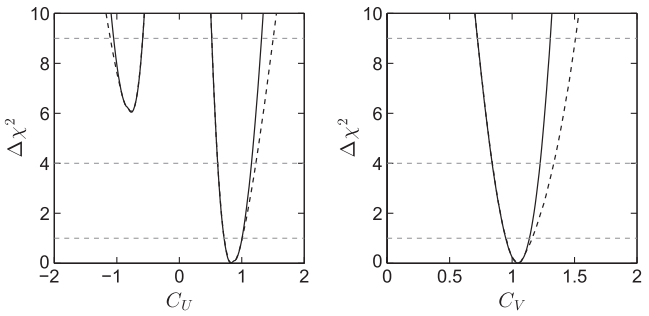

FIG. 4. Fit of C_U, C_D, C_V for $\Delta C_g = \Delta C_\gamma = 0$. The plots show the 1D $\Delta\chi^2$ distribution as a function of C_U (left) and C_V (right). The solid (dashed) lines are for the case that invisible/unseen decays are absent (allowed).

convention where m_t is positive—is quite problematic in the context of most theoretical models.[4] (We do not show the distribution for C_D here but just remark that $|C_D| \simeq 1 \pm 0.2$ with a sign ambiguity following from the weak dependence of the gg and $\gamma\gamma$ loops on the bottom-quark coupling.) For C_V, we find a best-fit value slightly above 1, at $C_V = 1.07$, but with the SM-like value of $C_V = 1$ lying well within 1 standard deviation.

Since $C_U < 0$ is now disfavored and the sign of C_D is irrelevant, we confine ourselves subsequently to C_U, $C_D > 0$. In Fig. 5 we show $\Delta\chi^2$ distributions in 2D planes confined to this range, still assuming $\Delta C_g = \Delta C_\gamma = 0$.

The mild correlation between C_U and C_D in the leftmost plot of Fig. 5 follows from the very SM-like signal rates in the VV and $\gamma\gamma$ final states in ggF: varying C_D implies a variation of the partial width $\Gamma(H \to bb)$, which dominates the total width. Hence, the branching fractions $\mathcal{B}(H \to VV)$ and $\mathcal{B}(H \to \gamma\gamma)$ change in the opposite direction, decreasing with increasing total width (i.e. with increasing C_D) and vice versa. To keep the signal rates close to 1, the ggF production cross section, which is roughly proportional to C_U^2, has to vary in the same direction as C_D.

The best fit is obtained for $C_U = 0.88$, $C_D = 0.94$, $C_V = 1.04$, $C_\gamma = 1.09$, $C_g = 0.88$ (and, in fact, $\mathcal{B}_{\rm inv} = 0$). Note that if $C_V > 1$ were confirmed, this would imply that the observed Higgs boson must have a significant triplet (or higher representation) component [71,72]. Currently the coupling fits are, however, perfectly consistent with SM values. Again, with a $\chi^2_{\rm min} = 17.79$ (for 20 d.o.f.) as compared to $\chi^2 = 18.95$ for the SM, allowing for deviations from the SM does not significantly improve the fit.

In models where the Higgs sector consists of doublets + singlets only one always obtains $C_V \leq 1$. Results for this case are shown in Fig. 6. Given the slight preference for $C_V > 1$ in the previous free-C_V plots, it is no surprise the $C_V = 1$ provides the best fit along with $C_U = C_g = 0.87$, $C_D = 0.88$ and $C_\gamma = 1.03$. Of course, the SM is again well within the 68% C.L. zone.

The general case of free parameters C_U, C_D, C_V, ΔC_g and ΔC_γ is illustrated in Fig. 7, where we show the 1D $\Delta\chi^2$ distributions for these five parameters (each time profiling over the other four parameters). As before, the solid (dashed) lines indicate results not allowing for (allowing for) invisible/unseen decay modes of the Higgs. Allowing for invisible/unseen decay modes again relaxes the $\Delta\chi^2$ behavior only modestly. The best-fit point always corresponds to $\mathcal{B}_{\rm inv} = 0$.

An overview of the current status of invisible decays is given in Fig. 8, which shows the behavior of $\Delta\chi^2$ as a function of $\mathcal{B}_{\rm inv}$ for various different cases of interest:

(a) SM Higgs with allowance for invisible decays—one finds $\mathcal{B}_{\rm inv} < 0.09\,(0.19)$;
(b) $C_U = C_D = C_V = 1$ but ΔC_γ, ΔC_g allowed for—$\mathcal{B}_{\rm inv} < 0.11\,(0.29)$;

[4]If the top quark and Higgs bosons are considered as fundamental fields, it would require that the top quark mass is induced dominantly by the vev of at least one additional Higgs boson, which is not the Higgs boson considered here, and typically leads to various consistency problems as discussed, e.g., in [70].

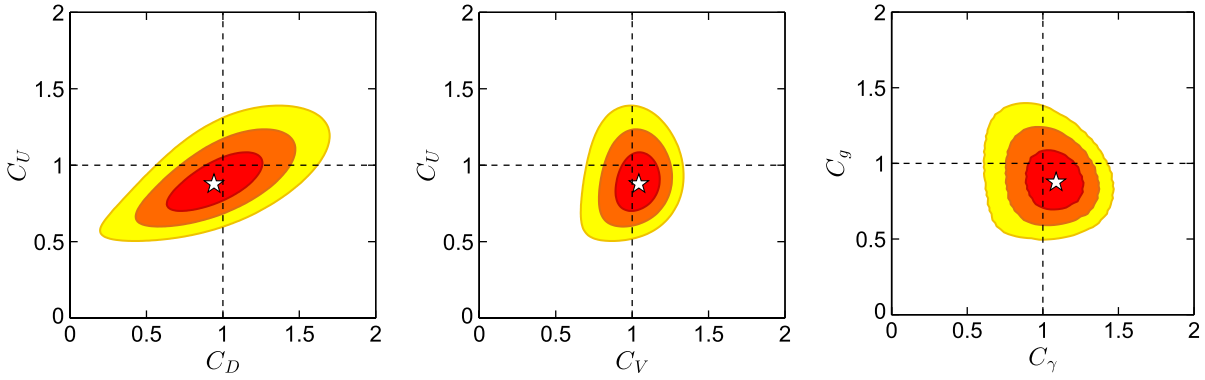

FIG. 5 (color online). Fit of $C_U > 0$, $C_D > 0$ and C_V for $\Delta C_g = \Delta C_\gamma = 0$. The red, orange and yellow areas are the 68%, 95% and 99.7% C.L. regions, respectively, assuming invisible decays are absent. The white star marks the best-fit point.

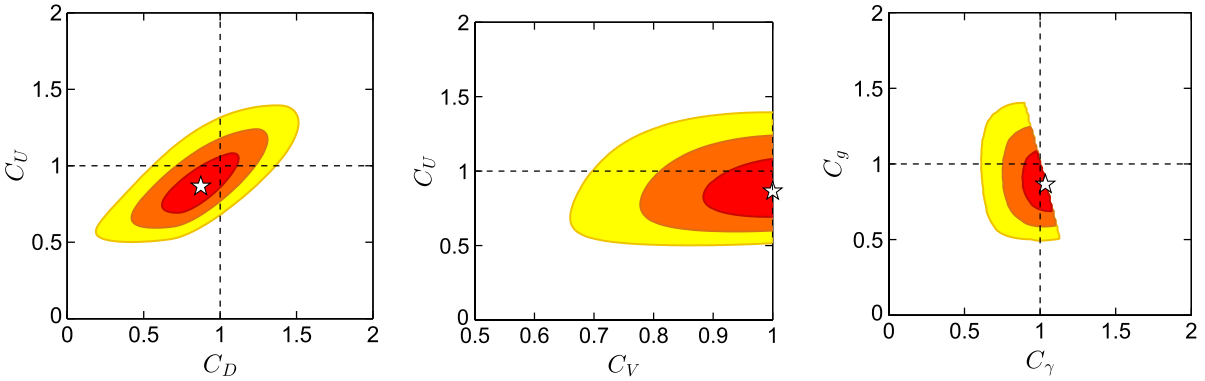

FIG. 6 (color online). As in Fig. 5 but for $C_V \leq 1$.

(c) C_U, C_D, C_V free, $\Delta C_\gamma = \Delta C_g = 0$,—$\mathcal{B}_{\rm inv} < 0.15\,(0.36)$;
(d) C_U, C_D free, $C_V \leq 1$, $\Delta C_\gamma = \Delta C_g = 0$—$\mathcal{B}_{\rm inv} < 0.09\,(0.24)$;
(e) C_U, C_D, C_V, ΔC_g, ΔC_γ free—$\mathcal{B}_{\rm inv} < 0.16\,(0.38)$.

[All $\mathcal{B}_{\rm inv}$ limits are given at 68% (95%) C.L.] Thus, while $\mathcal{B}_{\rm inv}$ is certainly significantly limited by the current data set, there remains ample room for invisible/unseen decays. At 95% C.L., $\mathcal{B}_{\rm inv}$ as large as ~0.38 is possible. Here, we remind the reader that the above results are obtained after fitting the 125.5 GeV data *and* inputting the experimental results for the $(Z \to \ell^+\ell^-)$ + invisible direct searches. When $C_V \leq 1$, $H \to$ invisible is much more constrained by the global fits to the H properties than by the direct searches for invisible decays; cf. the solid, dashed and dash-dotted lines in Fig. 8. For unconstrained C_U, C_D and C_V, on the other hand, cf. the dotted line and crosses in Fig. 8, the limit comes from the direct search for invisible decays in the ZH channel.

A comment is in order here. In principle there is a flat direction in the unconstrained LHC Higgs coupling fit when unobserved decay modes are present: setting $C_U = C_D = C_V \equiv C$, so that ratios of rates remain fixed, all the Higgs production × decay rates can be kept fixed to the SM ones by scaling up C while adding a new, unseen decay mode with branching ratio $\mathcal{B}_{\rm new}$ according to $C^2 = 1/(1 - \mathcal{B}_{\rm new})$ [73,74]; see also [75].[5] In [48] we found that it is mainly C_V that is critical here, because of the rather well measured VBF $\to H \to VV$ channel. Therefore limiting $C_V \leq 1$ gives a strong constraint on $\mathcal{B}_{\rm new}$, similar to the case of truly invisible decays. Concretely we find at 95% C.L.: (i) $\mathcal{B}_{\rm new} < 0.21$ for a SM Higgs with allowance for unseen decays; (ii) $\mathcal{B}_{\rm new} < 0.39$ for $C_U = C_D = C_V = 1$ but ΔC_γ, ΔC_g allowed for; and (iii) $\mathcal{B}_{\rm new} < 0.31$ for C_U, C_D free, $C_V \leq 1$ and $\Delta C_\gamma = \Delta C_g = 0$. For unconstrained C_U, C_D and C_V, however, there is no limit on $\mathcal{B}_{\rm new}$.

With this in mind, the global fit we perform here also makes it possible to constrain the Higgs boson's total decay width, $\Gamma_{\rm tot}$, a quantity that is not directly measurable at the LHC. For SM + invisible decays, we find $\Gamma_{\rm tot}/\Gamma_{\rm tot}^{\rm SM} < 1.11\,(1.25)$ at 68% (95%) C.L. Figure 9 shows the $\Delta\chi^2$ as a function of $\Gamma_{\rm tot}/\Gamma_{\rm tot}^{\rm SM}$ for the fits of C_U, C_D, and $C_V \leq 1$; C_U, C_D, and C_V free; and C_U, C_D, C_V, ΔC_g, ΔC_γ. The case of ΔC_g, ΔC_γ with $C_U = C_D = C_V = 1$ is not shown; without invisible decays we find $\Gamma_{\rm tot}/\Gamma_{\rm tot}^{\rm SM} = [0.98, 1.0]$ ([0.97, 1.02]) at 68% (95%) C.L. in this case. Allowing for invisible decays this changes to $\Gamma_{\rm tot}/\Gamma_{\rm tot}^{\rm SM} = [0.97, 1.14]$,

[5]We thank Heather Logan for pointing this out.

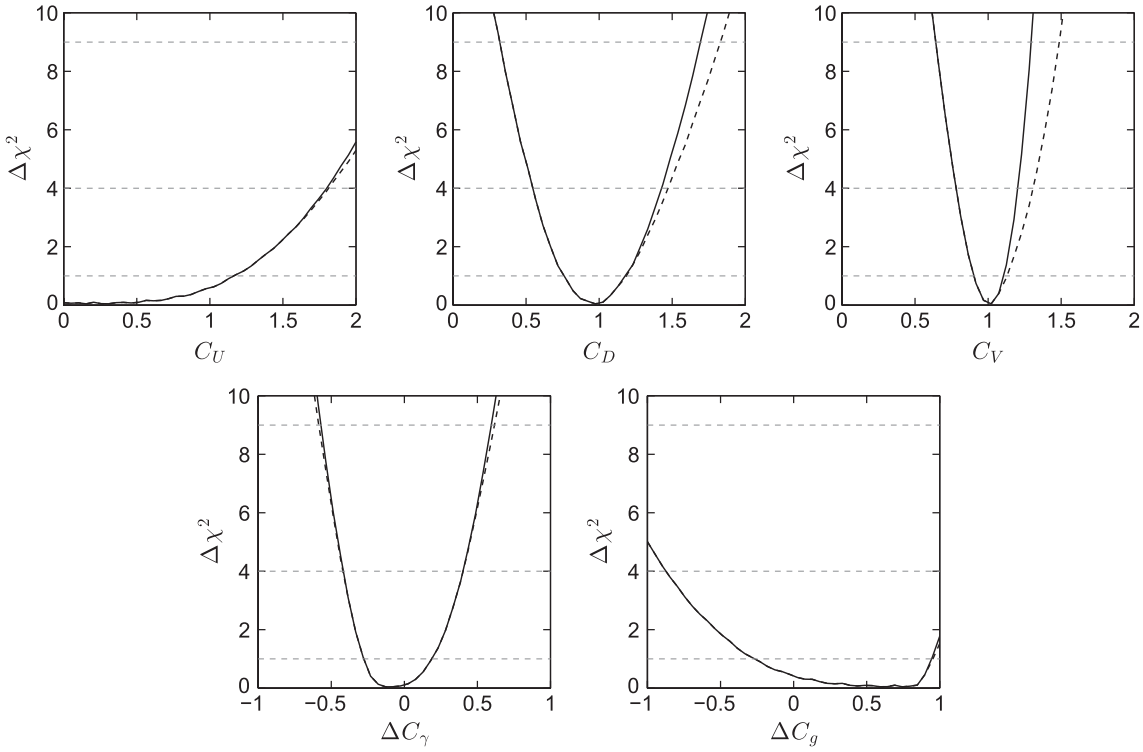

FIG. 7. Five (six) parameter fit of C_U, C_D, C_V, ΔC_g and ΔC_γ; the solid (dashed) curves are those obtained when invisible/unseen decay modes are not allowed (allowed) for.

([0.96, 1.46]); i.e. it is very close to the line for C_U, C_D, $C_V \leq 1$ in the right plot of Fig. 9.

IV. APPLICATION TO SPECIFIC MODELS

So far our fits have been largely model independent, relying only on assuming the Lagrangian structure of the SM. Let us now apply our fits to some concrete examples of specific models in which there are relations between some of the coupling factors C_I.

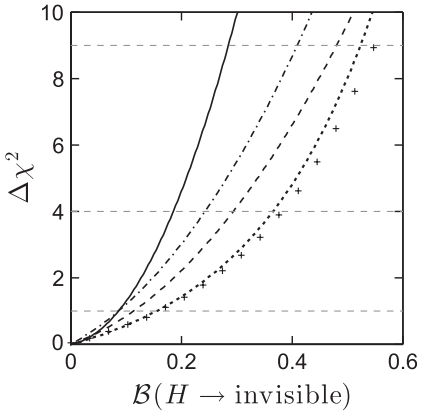

FIG. 8. $\Delta\chi^2$ distributions for the branching ratio of invisible Higgs decays for various cases. Solid curve: SM + invisible. Dashed curve: varying ΔC_g and ΔC_γ for $C_U = C_D = C_V = 1$. Dotted curve: varying C_U, C_D and C_V for $\Delta C_g = \Delta C_\gamma = 0$. Dot-dashed curve: varying C_U, C_D and $C_V \leq 1$ for $\Delta C_g = \Delta C_\gamma = 0$. Crosses: varying C_U, C_D, C_V, ΔC_g and ΔC_γ.

A. Two-Higgs-doublet models

As a first example, we consider two-Higgs-doublet models (2HDMs) of Type I and Type II (see also [47,76–84] for other 2HDM analyses in the light of recent LHC data). In both cases, the basic parameters describing the coupling of either the light h or the heavy H CP-even Higgs boson are only two: α (the CP-even Higgs mixing angle) and $\tan\beta = v_u/v_d$, where v_u and v_d are the vacuum

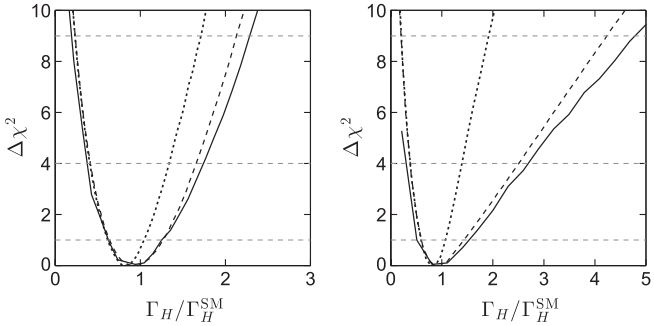

FIG. 9. $\Delta\chi^2$ distributions for the total Higgs decay width relative to SM, $\Gamma_{\rm tot}/\Gamma_{\rm tot}^{\rm SM}$, on the left without invisible decays, on the right including $\mathcal{B}_{\rm inv}$ as a free parameter in the fit. The lines are for C_U, C_D and $C_V \leq 1$ (dotted curve); C_U, C_D and free C_V (dashed curve); and C_U, C_D, free C_V, ΔC_g, ΔC_γ (solid curve).

TABLE II. Tree-level vector boson couplings C_V ($V = W, Z$) and fermionic couplings C_F normalized to their SM values for the two scalars h, H and the pseudoscalar A in Type I and Type II two-Higgs-doublet models.

	Type I and II	Type I		Type II	
Higgs	VV	Up quarks	Down quarks & leptons	Up quarks	Down quarks & leptons
h	$\sin(\beta-\alpha)$	$\cos\alpha/\sin\beta$	$\cos\alpha/\sin\beta$	$\cos\alpha/\sin\beta$	$-\sin\alpha/\cos\beta$
H	$\cos(\beta-\alpha)$	$\sin\alpha/\sin\beta$	$\sin\alpha/\sin\beta$	$\sin\alpha/\sin\beta$	$\cos\alpha/\cos\beta$
A	0	$\cot\beta$	$-\cot\beta$	$\cot\beta$	$\tan\beta$

expectation values of the Higgs field that couples to up-type quarks and down-type quarks, respectively. The Type I and Type II models are distinguished by the pattern of their fermionic couplings as given in Table II. The SM limit for the h (H) in the case of both Type I and Type II models corresponds to $\alpha = \beta - \pi/2$ ($\alpha = \beta$). We implicitly assume that there are no contributions from non-SM particles to the loop diagrams for C_γ and C_g. In particular, this means our results correspond to the case where the charged Higgs boson, whose loop might contribute to C_γ, is heavy.

The results of the 2HDM fits are shown in Fig. 10 for the case that the state near 125 GeV is the lighter CP-even h. To be precise, the top row shows $\Delta\chi^2$ contours in the β versus $\cos(\beta-\alpha)$ plane while the bottom row shows the 1D projection of $\Delta\chi^2$ onto $\cos(\beta-\alpha)$ with β profiled over. For identifying the heavier H with the state near 125 GeV, replace $\cos(\beta-\alpha)$ by $\sin(\beta-\alpha)$ in the 1D plots. (Since the ~125 GeV state clearly couples to WW, ZZ, we do not consider the case where the A is the only state at ~125 GeV.)

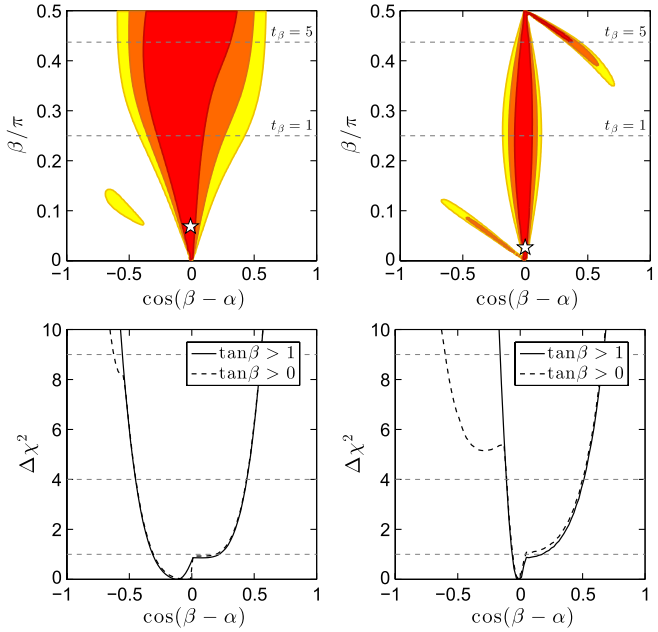

FIG. 10 (color online). Fits for the 2HDM Type I (left) and Type II (right) models for $m_h = 125.5$ GeV. See text for details.

In the case of the Type I model, we note a rather broad valley along the SM limit of $\cos(\beta-\alpha) = 0$, which is rather flat in $\tan\beta$; the 68% (95%) C.L. region extends to $\cos(\beta-\alpha) = [-0.31, 0.19]$ ($[-0.45, 0.44]$). The best-fit point lies at $\beta \simeq 0.02\pi$ and $\alpha \simeq 1.52\pi$ with $\chi^2_{\rm min} = 18.01$ for 21 d.o.f. (to be compared to the SM $\chi^2_{\rm min} = 18.95$). Requiring $\tan\beta > 1$, this moves to $\beta \simeq 0.25\pi$, i.e. $\tan\beta$ just above 1, with $\alpha \simeq 1.71\pi$ and $\chi^2_{\rm min} = 18.08$. At 99.7% C.L., there is also a small island at $\cos(\beta-\alpha) \approx -0.5$ and $\tan\beta < 1$, which corresponds to the $C_U < 0$ solution. (This is responsible for the splitting of the two lines at $\cos(\beta-\alpha) \lesssim -0.5$ in the 1D plot.)

In contrast, for the Type II model, we observe two narrow 68% C.L. valleys in the β versus $\cos(\beta-\alpha)$ plane, one along the SM solution with the minimum again very close to $\beta \approx 0$ and a second banana-shaped one with $\tan\beta \gtrsim 5$ (3) and $\cos(\beta-\alpha) \lesssim 0.4$ (0.6) at 68% (95%) C.L. This second valley is the degenerate solution with $C_D \approx -1$; it does not appear in Fig. 3 of [83] because there C_U, $C_D > 0$ was implicitly assumed. The best-fit point is very similar to that for Type I: $\beta \simeq 0.01\pi$ (0.25π) and $\alpha \simeq 1.5\pi$ (1.75π) with $\chi^2_{\rm min} = 18.68$ (18.86) for 21 d.o.f. for arbitrary $\tan\beta$ ($\tan\beta > 1$). Again, there is an additional valley very close to $\beta \sim 0$, extending into the negative $\cos(\beta-\alpha)$ direction, which, however, does not have a 68% C.L. region. In 1D, we find $\cos(\beta-\alpha) = [-0.11, 0.50]$ at 95% C.L.

Let us end the 2HDM discussion with some comments regarding the "other" scalar and/or the pseudoscalar A. To simplify the discussion, we will focus on the $m_h = 125.5$ GeV case. First, we note that if H and A are heavy enough (having masses greater than roughly 600 GeV), then their properties are unconstrained by LHC data and the global fits for the h will be unaffected. If they are lighter, then it becomes interesting to consider constraints that might arise from not having observed them. Such constraints will, of course, depend upon their postulated masses, both of which are independent parameters in the general 2HDM. For purposes of discussion, let us neglect the possibly very important $H, A \to hh$ decays. The most relevant final states are then $H \to VV$ and $H, A \to \tau\tau$.

With regard to observing the heavy Higgs in the $H \to VV$ channels, we note that for the H our fits predict the VV coupling to be very much suppressed in a large part

(but not all) of the 95% C.L. allowed region. While this implies suppression of the VBF production mode for the H, it does not affect the ggF production mode and except for very small VV coupling the branching ratio of the H to VV final states declines only modestly. As a result, the limits in the $ZZ \to 4\ell$ channel [7], which already extend down to about $0.1 \times$ SM in the mass range $m_H \approx$ 180–400 GeV, and to about $0.8 \times$ SM at $m_H \approx 600$ GeV, can be quite relevant. For instance, for a heavy scalar H of mass $m_H = 300$ GeV, in the 95% C.L. region of our fits the signal strength in the $gg \to H \to ZZ$ channel ranges from 0 to 5.4 in Type I and from 0 to 33 in Type II. For $m_H = 600$ GeV, we find $\mu(gg \to H \to ZZ) \lesssim 1.1\,(0.6)$ in Type I (II). Further, at the best-fit point for $\tan\beta > 1$, $\mu(gg \to H \to ZZ) = 1.10\,(0.08)$ at $m_H = 300\,(600)$ GeV in Type I and $\mu(gg \to H \to ZZ) = 0.12\,(0.001)$ at $m_H = 300\,(600)$ GeV in Type II, which violate the nominal limits at $m_H = 300$ GeV in both models. Note, however, that it is possible to completely evade the 4ℓ bounds if $H \to hh$ decays are dominant.

Moreover, both the H and the A, which has no tree-level couplings to VV, may show up in the $\tau\tau$ final state through ggF. Limits from ATLAS [85] range (roughly) from $\mu(gg \to H, A \to \tau\tau) < 2500$ at $m_{H,A} = 300$ GeV to <21000 at $m_{H,A} = 500$ GeV. These may seem rather weak limits, but in fact the signal strengths for $H \to \tau\tau$ and $A \to \tau\tau$ (relative to $H_{\rm SM}$) can be extremely large. In the case of the A, this is because the $A \to \tau\tau$ branching ratio is generically much larger than the $H_{\rm SM} \to \tau\tau$ branching ratio, the latter being dominated by VV final states at high mass. In the case of the H, the same statement applies whenever its VV coupling is greatly suppressed. We find that only the Type I model with $\tan\beta > 1$ completely evades the $\tau\tau$ bounds throughout the 95% C.L. region of the h fit since both the fermionic couplings of H and A are suppressed by large $\tan\beta$. In the Type II model, $gg \to A \to \tau\tau$ satisfies the $\tau\tau$ bounds at 95% C.L., but $gg \to H \to \tau\tau$ can give a very large signal. However, the best-fit h point for $\tan\beta > 1$ in Type II predicts $\mu(gg \to H \to \tau\tau)$ values of 674 and 6.4 at 300 and 500 GeV, both of which satisfy the earlier-stated bounds. We also stress that no bounds are available in the $\tau\tau$ channel above 500 GeV.

Clearly, a full study is needed to ascertain the extent to which limits in the $H \to ZZ$ and $H, A \to \tau\tau$ channels will impact the portion of the α-β plane allowed at 95% C.L. after taking into account Higgs-to-Higgs decays, which are typically substantial. This is beyond the scope of this paper and will be presented elsewhere [86].

B. Inert doublet model

In the Inert Doublet Model (IDM) [87], a Higgs doublet $\tilde{H}_2$ that is odd under a Z_2 symmetry is added to the SM leading to four new particles: a scalar $\tilde{H}$, a pseudoscalar $\tilde{A}$, and two charged states $\tilde{H}^\pm$ in addition to the SM-like Higgs h.[6] All other fields being even, this discrete symmetry not only guarantees that the lightest inert Higgs particle is stable, and thus a suitable dark matter candidate [88–91], but also prevents the coupling of any of the inert doublet particles to pairs of SM particles. Therefore, the only modification to the SM-like Higgs couplings is through the charged Higgs contribution to ΔC_γ. The scalar potential of the IDM is given by

$$V = \mu_1^2|H_1|^2 + \mu_2^2|\tilde{H}_2|^2 + \lambda_1|H_1|^4 + \lambda_2|\tilde{H}_2|^4 + \lambda_3|H_1|^2|\tilde{H}_2|^2 + \lambda_4|H_1^\dagger\tilde{H}_2|^2 + \frac{\lambda_5}{2}[(H_1^\dagger\tilde{H}_2)^2 + \text{H.c.}], \tag{2}$$

where $\mu_2^2 > -v^2$ is required in order that $\tilde{H}_2^0$ not acquire a nonzero vev (which would violate the symmetry needed for $\tilde{H}$ to be a dark matter particle). The crucial interactions implied by this potential are those coupling the light iggs h associated with the H_1 field to pairs of Higgs bosons coming from the $\tilde{H}_2$ field. These are given by $-(2m_W/g)\lambda_3 h\tilde{H}^+\tilde{H}^-$, $-(2m_W/g)\lambda_L h\tilde{H}\tilde{H}$ and $-(2m_W/g)\lambda_S h\tilde{A}\tilde{A}$ for the charged, scalar and pseudoscalar, respectively, where

$$\lambda_{L,S} = \frac{1}{2}(\lambda_3 + \lambda_4 \pm \lambda_5). \tag{3}$$

With these abbreviations, the Higgs masses at tree level can be written as

$$m_h^2 = \mu_1^2 + 3\lambda_1 v^2, \qquad m_{\tilde{H},(\tilde{A})}^2 = \mu_2^2 + \lambda_{L(S)}v^2, \qquad m_{\tilde{H}^\pm}^2 = \mu_2^2 + \frac{1}{2}\lambda_3 v^2. \tag{4}$$

Moreover, the couplings to the inert charged and neutral Higgses are related by

$$\frac{\lambda_3}{2} = \frac{1}{v^2}(m_{\tilde{H}^+}^2 - m_{\tilde{H}}^2) + \lambda_L. \tag{5}$$

It is important to note that *a priori* $m_{\tilde{H},\tilde{A},\tilde{H}^+}^2$ are each free parameters and could be small enough that h decays to a pair of the dark sector states would be present and possibly very important. The $h \to \tilde{H}\tilde{H}$ and $h \to \tilde{A}\tilde{A}$ decays would be invisible and contribute to $\mathcal{B}_{\rm inv}$ for the h; $h \to \tilde{H}^+\tilde{H}^-$ decays would generally be visible so long as the $\tilde{H}^+$ was not closely degenerate with the $\tilde{H}$.

Theoretical constraints impose some conditions on the couplings. Concretely, we assume a generic perturbativity upper bound $|\lambda_i| < 4\pi$, which, when coupled with the vacuum stability and perturbative unitarity conditions on the potential, leads to $\lambda_3 > -1.5$ and $\mu_2^2 \gtrsim -4.5 \times 10^4$ GeV^2 [91,92]. We also adopt a lower bound of $m_{\tilde{H}^\pm} > 70$ GeV, as derived from chargino limits at LEP [93,94].

[6]For distinction with the 2HDM, we denote all IDM particles odd under Z_2 with a tilde.

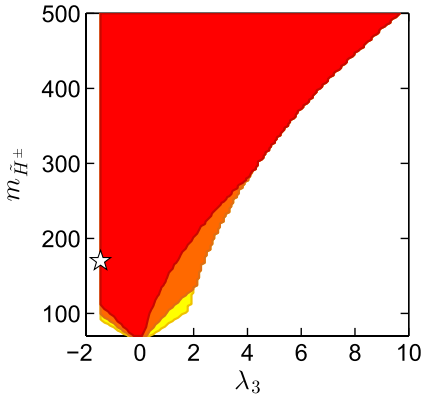

FIG. 11 (color online). Contours of 68%, 95%, 99.7% C.L. in the $m_{\tilde{H}^\pm}$ versus λ_3 plane for the IDM assuming that there are no invisible decays of the SM-like Higgs h.

Note, however, that LHC exclusions for the SM Higgs do not apply to members of the inert doublet because (i) they do not couple to fermions and (ii) trilinear and quartic couplings to gauge bosons involve two inert Higgses.

Let us now turn to the fit results.[7] First, we consider the case where $m_{\tilde{H}}, m_{\tilde{A}} > m_h/2$—the only deviation from the SM then arises from the charged Higgs contribution to ΔC_γ parametrized by λ_3 and $m_{\tilde{H}^\pm}$. The general one-parameter fit to the Higgs couplings leads to the bounds $-0.02\,(-0.13) < \Delta C_\gamma < 0.17\,(0.26)$ at 1σ (2σ). The corresponding contours in the $m_{\tilde{H}^\pm}$ versus λ_3 plane are shown in Fig. 11. Note that the third equality of Eq. (4) and the lower bound of $\mu_2^2 \gtrsim -4.5 \times 10^4$ GeV^2 imply an upper bound on λ_3 for any given $m_{\tilde{H}^\pm}$. This excludes the large-λ_3 region when $m_{\tilde{H}^+} \gtrsim 130$ GeV. The impact of the global fit is confined to the region $m_{\tilde{H}^+} \lesssim 130$ GeV and $|\lambda_3| \lesssim 2$ (at 95% C.L.). The best-fit point lies at $m_{\tilde{H}^+} = 170$ GeV and $\lambda_3 = -1.47$.

Second, we consider the case where the inert scalar is light and examine how invisible $h \to \tilde{H}\tilde{H}$ decays further constrain the parameters. The bounds on the invisible width actually lead to a strong constraint on the coupling λ_L. The 1σ (2σ) allowed range is roughly $\lambda_L \times 10^3 = \pm 4$ (± 7) for $m_{\tilde{H}} = 10$ GeV. This bound weakens only when the invisible decay is suppressed by kinematics; for $m_{\tilde{H}} = 60$ GeV, we find $\lambda_L \times 10^3 = [-9, 7]$ ($[-13, 12]$) at 1σ (2σ). The $\Delta\chi^2$ distributions of λ_L for $m_{\tilde{H}} = 10$ and 60 GeV are shown in the left panel in Fig. 12, with $m_{\tilde{H}^\pm}$ profiled over from 70 GeV to about 650 GeV (the concrete upper limit being determined by the perturbativity constraint). This strong constraint on λ_L implies that it can be neglected in Eq. (5) and that the charged Higgs coupling λ_3 is directly related to $m_{\tilde{H}^\pm}$ for a given $m_{\tilde{H}}$, as illustrated in the middle panel of Fig. 12 (here, the mass of the inert scalar is profiled over in the range $m_{\tilde{H}} \in [1, 60]$ GeV). As a result the value of C_γ is also strongly constrained from the upper bound on the invisible width. For example, for $m_{\tilde{H}} = 10$ GeV, we find that $C_\gamma = [0.940, 0.945]$ at 68% C.L. Note that because $m_{\tilde{H}^\pm} > m_{\tilde{H}}$ is needed in order to have a neutral dark matter candidate, λ_3 is always positive and therefore $C_\gamma < 1$. To approach $C_\gamma \simeq 1$, the inert Higgs mass has to be close to the kinematic threshold, $m_{\tilde{H}} \to m_h/2$ so that the constraint on λ_L is relaxed. For illustration, see the right panel of Fig. 12. These results imply that with an improved accuracy on the measurements of the Higgs coupling, for example showing that $C_\gamma > 0.95$, it would be possible to exclude light dark matter ($m_{\tilde{H}} < 10$ GeV) in the IDM. Another consequence is that for a given $m_{\tilde{H}}$ the perturbativity limit $\lambda_3 < 4\pi$ implies an upper bound on the charged Higgs mass. For $m_{\tilde{H}} \in [1, 60]$ GeV we obtain $m_{\tilde{H}^\pm} < 620$ GeV.

Finally note that the case where $\tilde{A}$ is the lightest neutral state and $m_{\tilde{A}} < m_h/2$ is analogous to the $\tilde{H}$ case just discussed, with $m_{\tilde{H}} \to m_{\tilde{A}}$ and $\lambda_L \to \lambda_S$, and leads to analogous conclusions. Analyses of the Higgs sector of the inert doublet model were also performed recently in [91,96–99].

C. Triplet Higgs model

In this section we consider the model of [100], which combines a single Higgs doublet field with $Y = 0$ and $Y = \pm 1$ triplet fields in such a way that custodial symmetry is preserved at tree level. The phenomenology of this model was developed in detail in [101,102]. In this model, the neutral doublet and triplet fields acquire vacuum expectation values given by $\langle\phi^0\rangle = a/\sqrt{2}$ and $\langle\chi^0\rangle = \langle\xi^0\rangle = b$, respectively. It is the presence of the two triplet fields and their neutral members having the same vev, b, that guarantees $\rho = 1$ at tree level. The value of $v^2 \equiv a^2 + 8b^2 = (246\ \text{GeV})^2$ is determined by the W, Z masses. However, the relative magnitude of a and b is a parameter of the model. The relative mixture is defined by the doublet-triplet mixing angle θ_H with cosine and sine given by $c_H = \frac{a}{\sqrt{a^2+8b^2}}$ and $s_H = \sqrt{\frac{8b^2}{a^2+8b^2}}$. The angle θ_H is reminiscent of the β angle of a 2HDM. Just like β, θ_H can be taken to lie in the first quadrant so that both c_H and s_H are positive.

In this model, it is most natural to choose a Higgs sector potential that preserves the custodial symmetry. In this case, the Higgs eigenstates comprise a five-plet, a triplet and two singlets, H_1^0 and $H_1^{0\prime}$. The Higgs bosons of the five-plet couple only to vector boson pairs and those of the triplet couple only to fermion pairs. Further, the neutral members of the five-plet and the triplet cannot mix (without violating the custodial symmetry). As a result, they cannot describe the Higgs-boson–like state seen at the LHC. In contrast, the H_1^0 and $H_1^{0\prime}$ can mix. Further, their reduced couplings are given by

[7] In our IDM fits, the $h\gamma\gamma$ coupling is computed with MICROMEGAS 3 [95].

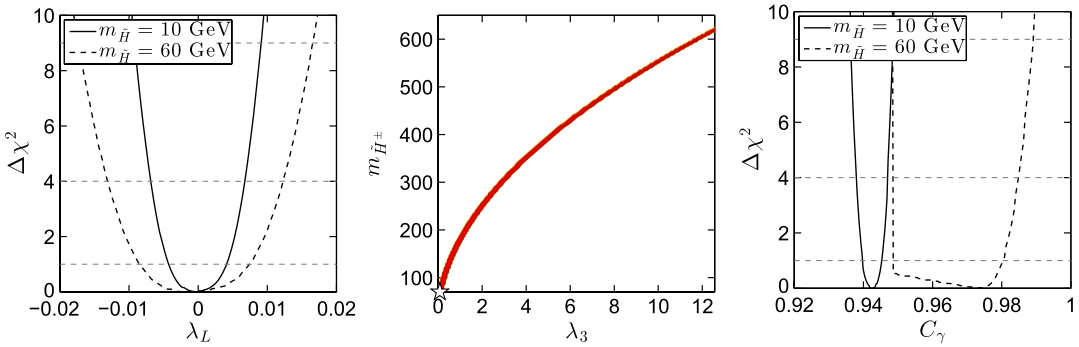

FIG. 12 (color online). Left panel: $\Delta\chi^2$ distribution of λ_L for $m_{\tilde{H}} = 10$ GeV (full line) and 60 GeV (dashed line) with $m_{\tilde{H}^+}$ profiled over its whole allowed range. Middle panel: relation between $m_{\tilde{H}^\pm}$ and λ_3 with $m_{\tilde{H}}$ profiled over from 1 to 60 GeV. Right panel: $\Delta\chi^2$ as a function of C_γ for $m_{\tilde{H}} = 10$ GeV (full line) and 60 GeV (dashed line) with $m_{\tilde{H}^\pm}$ profiled over.

$$C_F(H_1^0) = \frac{1}{c_H}, \qquad C_V(H_1^0) = c_H,$$
$$C_F(H_1^{0\prime}) = 0, \qquad C_V(H_1^{0\prime}) = \frac{2\sqrt{2}}{\sqrt{3}} s_H, \tag{6}$$

where all fermionic couplings scale with the common factor C_F. We see that in the limit $c_H \to 1$ the H_1^0 looks exactly like the SM Higgs boson and the $H_1^{0\prime}$ has no tree-level couplings. More generally, from these expressions, it is clear that only a Higgs state that is primarily H_1^0 can provide the SM-like signal rates that typify the $\sim$125.5 GeV state observed at the LHC.

The mixing of the H_1^0 and $H_1^{0\prime}$ is determined by the mass-squared matrix,

$$\mathcal{M}^2_{H_1^0, H_1^{0\prime}} = \begin{pmatrix} c_H^2 \bar{\lambda}_{13} & s_H c_H \bar{\lambda}_3 \\ s_H c_H \bar{\lambda}_3 & s_H^2 \bar{\lambda}_{23} \end{pmatrix} v^2, \tag{7}$$

where we have defined

$$\bar{\lambda}_{13} \equiv 8(\lambda_1 + \lambda_3), \qquad \bar{\lambda}_{23} \equiv 3(\lambda_2 + \lambda_3), \qquad \bar{\lambda}_3 \equiv 2\sqrt{6}\lambda_3, \tag{8}$$

where $\lambda_{1,2,3}$ are couplings appearing in the full Higgs sector potential (see [101]), with $\lambda_1 + \lambda_3 > 0$ and $\lambda_2 + \lambda_3 > 0$ required for stability in the asymptotic ϕ and χ directions, respectively, and $\lambda_1\lambda_2 + \lambda_1\lambda_3 + \lambda_2\lambda_3 > 0$ required for positive mass squared for the mass eigenstates coming from the H_1^0-$H_1^{0\prime}$ sector. Clearly, the mixing between H_1^0 and $H_1^{0\prime}$ vanishes in the limit of $\lambda_3 \to 0$. More generally, the above mass-squared matrix will be diagonalized by a rotation matrix specified by an angle for which we use the 2HDM-like notation, α. We define α using the convention in which the Higgs boson mass eigenstates are given by

$$H = \cos\alpha H_1^0 + \sin\alpha H_1^{0\prime},$$
$$H' = -\sin\alpha H_1^0 + \cos\alpha H_1^{0\prime}. \tag{9}$$

We can solve for the $\bar{\lambda}$'s in terms of m_H^2 and $m_{H'}^2$ and the mixing angle α,

$$\bar{\lambda}_{13} = \frac{m_H^2 c_\alpha^2 + m_{H'}^2 s_\alpha^2}{c_H^2 v^2}, \qquad \bar{\lambda}_{23} = \frac{m_H^2 s_\alpha^2 + m_{H'}^2 c_\alpha^2}{s_H^2 v^2},$$
$$\bar{\lambda}_3 = \frac{(m_H^2 - m_{H'}^2) s_\alpha c_\alpha}{c_H s_H v^2}, \tag{10}$$

valid regardless of the relative size of m_H^2 and $m_{H'}^2$.

As regards the masses of the triplet members and of the five-plet members, we have degeneracy at tree level within the two representations with

$$m^2_{H_5} = 3(\lambda_5 s_H^2 + \lambda_4 c_H^2) v^2, \qquad m^2_{H_3} = \lambda_4 v^2, \tag{11}$$

implying that these masses can be chosen independently of the H_1^0-$H_1^{0\prime}$ sector.

The couplings of the H relative to the SM are

$$C_F = \frac{\cos\alpha}{c_H}, \qquad C_V = c_H \cos\alpha + \frac{2\sqrt{2}}{\sqrt{3}} s_H \sin\alpha. \tag{12}$$

Note that if s_H is sizable, then C_V will be enhanced relative to the SM value of 1 and the fermonic couplings will also be enhanced. As noted earlier, the angle θ_H can be chosen to be in the first quadrant: $0 \le \theta_H \le \pi/2$. For a full range of possible phenomenology, we must explore $0 \le \alpha \le 2\pi$. In passing, we note that if we require $C_F = 1$, then $\cos\alpha = c_H$, and plugging into the expression for C_V we find that $c_H^2 = 1$ is required if we demand also that $C_V = 1$.

The interesting question we want to answer is what does the LHC data allow for θ_H and α. The result is shown in Fig. 13, on the left in the θ_H versus α plane and on the right in the C_V versus C_F plane. As expected, the preferred region lies at small α and small θ_H, roughly $\alpha \in [0, \pi/4]$ and $\theta_H \in [0, 0.1\pi]$, leading to a very SM-like picture in the C_V versus C_F plane.

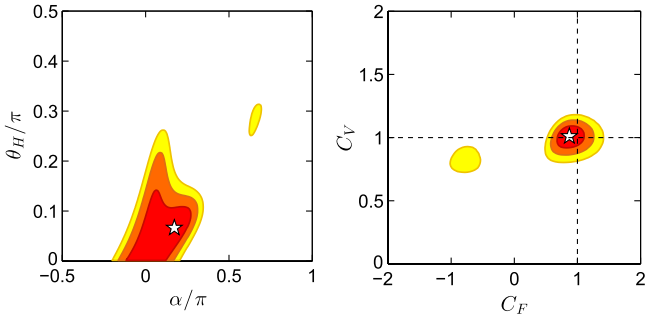

FIG. 13 (color online). Fit for the Georgi-Machacek triplet model [100] assuming that $H = \cos\alpha H_1^0 + \sin\alpha H_1^{0\prime}$ is the observed state at 125.5 GeV. (The right plot is also valid for 2HDMs of Type I.) See text for details.

At the best-fit point, $\alpha \sim 0.2\pi$, $\theta_H \sim 0.07\pi$, and taking $m_{H'} = m_H/2$ (so as to avoid $H \to H'H'$ decays; see below), we find

$$\bar{\lambda}_{13} \sim 0.21, \qquad \bar{\lambda}_{23} \sim 2.93, \qquad \bar{\lambda}_3 \sim 0.42, \quad (13)$$

perfectly consistent with the vacuum stability conditions given earlier and with perturbativity for the couplings themselves. As $m_{H'}$ increases, $\bar{\lambda}_{23}$ increases (when holding α and θ_H at their best-fit values). For example, at $m_{H'} = 400$ GeV, we have $\bar{\lambda}_{13} = 1.14$, $\bar{\lambda}_{23} = 38.25$ and $\bar{\lambda}_3 = -5.32$. From Eq. (8) we see that this is still within the perturbative limits defined as $|\lambda_i| < 4\pi$.

We have seen that the SM-like nature of the observed 125.5 GeV state requires small θ_H and α, implying that the H state will be mostly H_1^0 and that the H' state will be mostly $H_1^{0\prime}$. Further, from Eq. (7) and the above results for the $\bar{\lambda}_i$ we see that it is most natural for the mass of the H' to be smaller than the mass of the H for moderate values of the λ_i. This brings up the possibility that $H \to H'H'$ decays could be possible. If present, they would significantly deplete the SM decay modes of the H and the fit to the data would be bad. The $HH'H'$ coupling is given by [using Eq. (2.21) of [101] and the notation $c_\alpha \equiv \cos\alpha$, $s_\alpha \equiv \sin\alpha$]

$$-2HH'^2[4\lambda_3 c_\alpha^3 c_H + 4[9(\lambda_1+\lambda_3) - 2\lambda_3]c_\alpha c_H s_\alpha^2 + \sqrt{6}\lambda_3 c_H s_\alpha^3 - \sqrt{6}\lambda_3 c_\alpha^2 s_\alpha(2c_H - 9s_H)]v. \quad (14)$$

At the best-fit point, the coefficient of HH'^2 is $\sim -0.57v$ for $m_{H'} = m_H/2$, falling slowly as $m_{H'}$ decreases. Since this is a large coupling, $\mathcal{B}(H \to H'H')$ would be large at the best-fit point if this decay is allowed. Thus, our fitting results must be taken to apply only to the situation where $m_{H'} > m_H/2$. As discussed above, this presents no particular problem in the context of the model.

There are also couplings of the H to pairs of five-plet or triplet members [Eq. (2.22) of [101]]. Thus, to avoid the associated decays of the H we need to require $m_{H_5} > m_H/2$ and $m_{H_3} > m_H/2$, as Eq. (11) shows is easily arranged for appropriate choices of (the independent parameters) λ_4 and λ_5. In fact, experimental limits on the charged Higgs members of the five-plet and triplet from LEP [103] are of order 80 GeV and from LHC of order 120 GeV [104] assuming decay to $\tau^+\nu$. Limits on the doubly charged Higgs of the five-plet from the LHC [105] are of order 300 GeV (for decays to two charged leptons). Thus it seems certain that the (degenerate) masses of all the five-plet and all the triplet Higgses are necessarily $> m_H/2$. Note that this automatically means that the $H \to H_3^0 Z$ and $H \to H_3^\pm W^\mp$ decays that could be significant [see Eq. (2.15) of [101]] will also be forbidden.

Of course, it is certainly interesting to consider the H' itself. Its couplings relative to the SM are

$$C'_F = -\frac{\sin\alpha}{c_H}, \qquad C'_V = \frac{2\sqrt{2}}{\sqrt{3}} s_H \cos\alpha - c_H \sin\alpha. \quad (15)$$

For small α and θ_H, both will be small—the H' will be weakly coupled to both fermions and vector bosons. This is illustrated by plotting the preferred regions in the C'_V versus C'_F plane, displayed in Fig. 14 (where we are assuming, as above, that $H \to H'H'$ decays are forbidden).

In the mass region $m_{H'} \in [m_H/2, m_H]$ only LEP2 data could potentially yield direct constraints on the H'. For the lower portion of this mass range, $e^+e^- \to Z^* \to ZH'$ limits are significant and would eliminate some portion of the larger $|C'_V|$ region of Fig. 14. Using Table 14 of [106] and noting that $\mathcal{B}(H' \to b\bar{b})$ will be approximately the same as for a SM Higgs boson, we see that C'^2_V is limited to $\lesssim 0.028$ at $m_{H'} \sim 63$ GeV rising to $\lesssim 0.044$ at $m_{H'} = 80$ GeV and $\lesssim 0.24$ at $m_{H'} = 100$ GeV. Thus, for the plot of Fig. 14 to not conflict with LEP2 95% C.L. limits over the full 68% (95%) C.L. regions of the plot would require $m_{H'} > 100$ GeV (> 112 GeV). For the best-fit point, the LEP constraints are obeyed so long as $m_{H'} > 85$ GeV.

The fact that the $H'H_3^0Z$ coupling is large (in fact, enhanced) for small θ_H will imply constraints coming

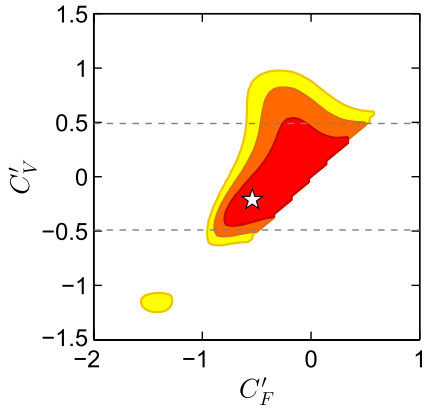

FIG. 14 (color online). Fit of C'_V versus C'_F of the H' in the Georgi-Machacek triplet Higgs model with $m_H = 125.5$ GeV. The regions above and below the dashed lines are excluded by LEP constraints for $m_{H'} = 100$ GeV.

from $e^+e^- \to Z^* \to H'H_3^0$ on the lower H' masses should m_{H_3} be small enough. For the $m_{H'} = 85$ GeV lower bound associated with the best-fit point (see above), Table 18 of [106] shows that $m_{H_3} > 110$ GeV is required, whereas for $m_{H'}$ close to m_H, there are no constraints for any $m_{H_3} > m_H/2$. In any case, all such constraints are avoided if m_{H_3} is above m_H, as easily arranged given Eq. (11), and almost guaranteed given the strong limits on its degenerate charged Higgs partner discussed above.

Of course, to avoid LEP2 limits on the H' the easiest choice is to take $m_{H'} > m_H$. In this region, LHC constraints derived from the $ZZ \to 4\ell$ channel must be examined. To do so, we need to first recall that $\mu(X \to H \to 4\ell)$ scales as $C_X^2\mathcal{B}(H \to ZZ)/\mathcal{B}(H_{\rm SM} \to ZZ)$, where $X =$ ggF or VBF. Even though $C_V'^2$ is typically suppressed, e.g. $C_V'^2 \sim 0.06$ at the best-fit point for the H, since both the partial width and total width are typically dominated by the VV final state $\mathcal{B}(H \to ZZ)/\mathcal{B}(H_{\rm SM} \to ZZ)$ is typically of order 1. In this approximation $\mu(\text{VBF} \to H' \to ZZ)$ will be suppressed because of the suppressed $C_V'^2$ and $\mu(\text{ggF} \to H' \to ZZ)$ will be suppressed by the small $C_F'^2$ values. Thus, except for the large C_V' region of Fig. 14, we expect that the LHC bounds are satisfied for any $m_{H'} > m_H$. Further, $H' \to 4\ell$ estimates should also take into account $H' \to HH$ decays, present when $m_{H'} > 2m_H$. These decays would deplete the 4ℓ channel, making it easier to satisfy the 4ℓ constraints. LHC constraints on the HH-type final state are not currently available from ATLAS and CMS. Finally, the $H' \to \tau\tau$ partial width will not be enhanced in this model since $|C_F'| < 1$ (see Fig. 14). Coupled with the reduced ggF rate, this will mean (unlike the 2HDM models) that the constraints from this channel will not impact the 95% C.L. region of the H fit even before allowing for $H' \to HH$ decays.

V. CONCLUSIONS

Using all publicly available results from the LHC and Tevatron experiments, we determined the combined likelihood ellipses for the Higgs signal around 125.5 GeV in the (ggF + ttH) versus (VBF + VH) production plane for various independent final states: $\gamma\gamma$, ZZ, WW, $\tau\tau$ and $b\bar{b}$. We presented parametrizations of these ellipses that should be of general utility for exploring different types of models.

Any model in which the Lagrangian structure has a SM-like form can be parametrized via scaling factors, C_U, C_D and C_V, for the up-quark, down-quark, lepton and vector boson couplings (relative to SM values), respectively. Additional new physics contributions to the one-loop gluon and photon couplings can be allowed for by writing scaling factors for the gg and $\gamma\gamma$ couplings in the form $C_g = \bar{C}_g + \Delta C_g$ and $C_\gamma = \bar{C}_\gamma + \Delta C_\gamma$ where the $\bar{C}_{g,\gamma}$ values are those predicted for given C_U, C_D and C_V using SM particle loops only. We can also allow for invisible/unseen decay modes of the Higgs by adding an invisible component to Higgs decays parametrized by $\mathcal{B}_{\rm inv}$. In terms of these input parameters, the χ^2 associated with each ellipse can be calculated. In this way, we were able to explore the behavior of the total χ^2 as a function of any one parameter (profiling over the other parameters that were allowed to vary freely in a given case) and also to determine the 68%, 95% and 99.7% contours in various 2D planes of any two of the freely varying parameters.

The most general fits considered were those in which C_U, C_D, C_V, ΔC_g, ΔC_γ were all allowed to vary freely. If there are no unseen (as opposed to truly invisible) decay modes of the Higgs, one finds that the observed 125.5 GeV state prefers to have quite SM-like couplings whether or not $\mathcal{B}_{\rm inv} = 0$ is imposed—more constrained fits, for example taking $\Delta C_g = \Delta C_\gamma = 0$ while allowing C_U, C_D, C_V to vary, inevitably imply that the other parameters must lie even closer to their SM values.

Allowing for invisible decays of the 125.5 GeV state through $\mathcal{B}_{\rm inv} > 0$ does not change the best-fit parameter values but does widen the $\Delta\chi^2$ distributions somewhat leading to important implications, e.g., for decays into dark matter particles. In particular, we found that at 95% C.L. there is still considerable room for such Higgs decays, up to $\mathcal{B}_{\rm inv} \sim 0.38$ when C_U, C_D, C_V, ΔC_g, ΔC_γ are all allowed to vary independently of one another. In comparison, a fit for which C_U, C_D are allowed to vary freely, but $C_V \leq 1$ is required (as appropriate for any doublets +singlets model) and $\Delta C_g = \Delta C_\gamma = 0$ is imposed, yields $\mathcal{B}_{\rm inv} \lesssim 0.24$ at 95% C.L. Even requiring completely SM couplings for the Higgs ($C_U = C_D = C_V = 1$, $\Delta C_g = \Delta C_\gamma = 0$) still allows $\mathcal{B}_{\rm inv} \leq 0.19$ at 95% C.L. It is worthwhile noting that for $C_V \leq 1$, the limits on $\mathcal{B}_{\rm inv}$ from global coupling fits are currently more constraining than those from direct searches for invisible decays, e.g., in the $ZH \to \ell^+\ell^- + E_T^{\rm miss}$ mode; thus for $C_V \leq 1$ the limits on merely unseen (i.e. not strictly invisible) decays are similar to the ones on $\mathcal{B}_{\rm inv}$.

As part of the fitting procedure, the total width of the Higgs relative to the SM prediction is computed as a function of the parameters and a $\Delta\chi^2$ distribution for $\Gamma_{\rm tot}/\Gamma_{\rm tot}^{\rm SM}$ is obtained. Assuming no unseen, but potentially visible, decays, we found $\Gamma_{\rm tot}/\Gamma_{\rm tot}^{\rm SM} \in [0.5, 2]$ at 95% C.L. for the case where C_U, C_D, C_V, ΔC_g, ΔC_γ and $\mathcal{B}_{\rm inv}$ are all allowed to vary freely, while $\Gamma_{\rm tot}/\Gamma_{\rm tot}^{\rm SM} \in [1, 1.25]$ at 95% C.L. if $C_U = C_D = C_V = 1$, $\Delta C_g = \Delta C_\gamma = 0$ are imposed and only $\mathcal{B}_{\rm inv} \geq 0$ is allowed for. These are useful limits given the inability to directly measure $\Gamma_{\rm tot}$ at the LHC. Of course, if there are unseen (but not invisible) decays, there is a flat direction that would prevent setting limits on the total width.

In the second part of the paper, we then examined implications of these results in the context of some simple concrete models with an extended Higgs sector: the Type I and Type II two-Higgs-doublet models; the inert doublet model; and the custodially symmetric triplet Higgs model.

Concretely, we used the combined likelihood ellipses to constrain the parameter spaces with corresponding implications for the properties of the other Higgs boson(s) of the model. In particular, the ability to discover a second neutral Higgs boson with mass above 125.5 GeV in, e.g., the 4ℓ mode can be quantified.

In the 2HDM, enhancement of the signal strength for a second neutral (scalar or pseudoscalar) Higgs boson with mass above 125.5 GeV can occur in both the 4ℓ and $\tau\tau$ channels. Therefore additional constraints on α and β can be set unless the decay of the heavier Higgs to a pair of the 125.5 GeV states dominates. Generally the signals in both channels can be at a level of interest for future LHC runs. In the triplet model, when the second Higgs, H', is heavy, the LHC bounds in both the $H' \to 4\ell$ and $H' \to \tau\tau$ channels are generally satisfied even without taking into account the heavy Higgs decays into pairs of 125.5 GeV Higgses. Only the region of parameter space with large C'_V requires a large branching fraction into Higgs pairs to deplete the 4ℓ signal. We stress that in both these models the heavy Higgs to Higgs pair decays are generically important when allowed, implying that ways must be found to be sensitive to the $4b$, $b\bar{b}\tau\tau$ and 4τ final states resulting therefrom.

In the inert doublet model, the inert Higgs states can only be pair produced and therefore are not currently constrained. However, we showed that the bound on the invisible decay of the 125.5 GeV SM-like Higgs, relevant when one inert Higgs is lighter than ≈ 60 GeV, constrains the allowed range for the two-photon width. Thus, a precise determination of C_γ could rule out light inert Higgs dark matter.

ACKNOWLEDGMENTS

This work originated from the workshops "Implications of the 125 GeV Higgs boson," which was held March 18–22, 2013 at LPSC Grenoble, and "The LHC Higgs Signal: Characterization, Interpretation and BSM Model Implications," held April 22–26, 2013, at UC Davis. Partial support by U.S. DOE Grant No. DE-FG03-91ER40674 and by IN2P3 under Contract PICS FR–USA No. 5872 is gratefully acknowledged. G. B., B. D., and S. K. acknowledge partial support from the French ANR DMAstroLHC. U. E. acknowledges partial support from the French ANR LFV-CPV-LHC, ANR STR-COSMO and the European Union FP7 ITN INVISIBLES (Marie Curie Actions, PITN-GA-2011-289442).

APPENDIX A: COMBINING LIKELIHOODS OF DIFFERENT EXPERIMENTS IN THE GAUSSIAN APPROXIMATION

As a function of the model-dependent signal rates μ_i [where i stands for $\gamma\gamma$, $VV^{(*)}$, $b\bar{b}$ and $\tau\tau$ (or $b\bar{b} = \tau\tau$)], the likelihoods in the Gaussian approximation in the $\mu(\text{ggF} + \text{ttH})$ versus $\mu(\text{VBF} + \text{VH})$ plane obtained by the experiment j (where j stands for ATLAS, CMS or the Tevatron) can be expressed as $\chi^2_{i,j}$ with

$$\begin{aligned}\chi^2_{i,j} &= a_{i,j}(\mu_i^{\text{ggF}} - \hat{\mu}_{i,j}^{\text{ggF}})^2 + 2b_{i,j}(\mu_i^{\text{ggF}} - \hat{\mu}_{i,j}^{\text{ggF}}) \\ &\quad \times (\mu_i^{\text{VBF}} - \hat{\mu}_{i,j}^{\text{VBF}}) + c_{i,j}(\mu_i^{\text{VBF}} - \hat{\mu}_{i,j}^{\text{VBF}})^2 \\ &\equiv a_{i,j}(\mu_i^{\text{ggF}})^2 + c_{i,j}(\mu_i^{\text{VBF}})^2 + 2b_{i,j}\mu_i^{\text{ggF}}\mu_i^{\text{VBF}} \\ &\quad + d_{i,j}\mu_i^{\text{ggF}} + e_{i,j}\mu_i^{\text{VBF}} + \cdots, \end{aligned} \tag{A1}$$

where $\hat{\mu}_{i,j}^{\text{ggF}}$ and $\hat{\mu}_{i,j}^{\text{VBF}}$ denote the best-fit points of the experiment j.[8] The dots denote terms independent of μ_i, which are irrelevant for χ^2_i relative to the best-fit points as defined in Eq. (1). $d_{i,j}$ and $e_{i,j}$ are given by

$$\begin{aligned} d_{i,j} &= -2a_{i,j}\hat{\mu}_{i,j}^{\text{ggF}} - 2b_{i,j}\hat{\mu}_{i,j}^{\text{VBF}}, \\ e_{i,j} &= -2c_{i,j}\hat{\mu}_{i,j}^{\text{VBF}} - 2b_{i,j}\hat{\mu}_{i,j}^{\text{ggF}}. \end{aligned} \tag{A2}$$

Combining experiments leads to

$$\begin{aligned}\chi^2_i &= a_i(\mu_i^{\text{ggF}})^2 + c_i(\mu_i^{\text{VBF}})^2 + 2b_i\mu_i^{\text{ggF}}\mu_i^{\text{VBF}} \\ &\quad + d_i\mu_i^{\text{ggF}} + e_i\mu_i^{\text{VBF}}, \end{aligned} \tag{A3}$$

with

$$\begin{aligned} a_i &= \sum_j a_{i,j}, \qquad b_i = \sum_j b_{i,j}, \qquad c_i = \sum_j c_{i,j}, \\ d_i &= \sum_j d_{i,j}, \qquad e_i = \sum_j e_{i,j}. \end{aligned} \tag{A4}$$

From (A3) one obtains Eq. (1) with

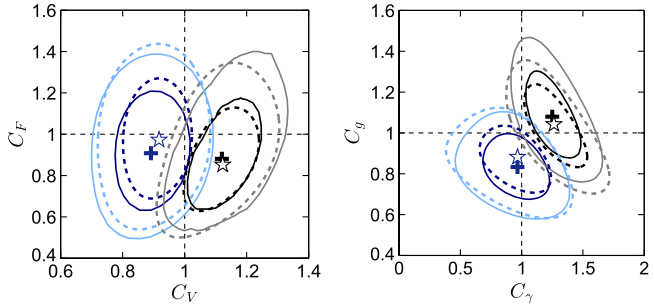

FIG. 15 (color online). Fit to the couplings (C_F, C_V) (left) and (C_g, C_γ) (right) using separately results from ATLAS and CMS up to the Moriond 2013 conference. The black and grey (dark blue and light blue) contours show the 68% and 95% C.L. regions for ATLAS (CMS), respectively. The solid contours correspond to the results published by the experimental collaborations, while dashed contours have been obtained using the fitted signal strength ellipses as determined using the separate data for ATLAS (CMS) in the manner described in Sec. II.

[8]Of course $\chi^2_{i,j}$ defined in this way is not an absolute χ^2, but rather a $\Delta\chi^2$ relative to the best-fit value of the experiment in a given channel.

$$\hat{\mu}_i^{\mathrm{ggF}} = \frac{b_i e_i - c_i d_i}{2(a_i c_i - b_i^2)}, \qquad \hat{\mu}_i^{\mathrm{VBF}} = \frac{b_i d_i - a_i e_i}{2(a_i c_i - b_i^2)}. \tag{A5}$$

APPENDIX B: COMPARISON WITH ATLAS AND CMS COUPLINGS FITS

Coupling fits using all available results up to the Moriond 2013 conference have been performed individually by ATLAS and CMS [3,4]. While the present paper aims at presenting combined results from ATLAS, CMS and Tevatron using parametrizations motivated by various models of new physics, the coupling fits made by ATLAS and CMS that combine the information from different channels can be used to check the robustness of the implementation of the experimental searches as presented in Sec. II. In particular, deviations of our results from those obtained by the ATLAS and/or CMS give a measure for the importance of the missing correlations mentioned at the end of Sec. I.

For the aim of comparison, we have performed fits to the (C_F, C_V) and (C_g, C_γ) couplings, using separately only ATLAS or CMS data up to the Moriond 2013 conference. Figure 15 compares our results to those published by ATLAS [4] and CMS [3]. We obtain good agreement in all four cases. The ATLAS (CMS) best-fit points are at distances of $\sqrt{(\Delta C_V)^2 + (\Delta C_F)^2} = 0.03$ (0.07) and $\sqrt{(\Delta C_\gamma)^2 + (\Delta C_g)^2} = 0.04$ (0.05) from the reconstructed best-fit points, and good coverage of the 68% and 95% C.L. regions is observed.

For completeness, we note that our fit for (C_F, C_V) combining ATLAS and CMS results up to the LHCP 2013 conference can be seen in the right plot of Fig. 13, and the one for (C_g, C_γ) in the middle plot in Fig. 3, taking $C_{g,\gamma} = 1 + \Delta C_{g,\gamma}$.

[1] G. Aad *et al.* (ATLAS Collaboration), Phys. Lett. B **716**, 1 (2012).
[2] S. Chatrchyan *et al.* (CMS Collaboration), Phys. Lett. B **716**, 30 (2012).
[3] CMS Collaboration, Report No. CMS-PAS-HIG-13-005, 2013.
[4] ATLAS Collaboration, Report No. ATLAS-CONF-2013-034, 2013.
[5] ATLAS Collaboration, Report No. ATLAS-CONF-2013-011, 2013.
[6] ATLAS Collaboration, Report No. ATLAS-CONF-2013-012, 2013.
[7] ATLAS Collaboration, Report No. ATLAS-CONF-2013-013, 2013.
[8] ATLAS Collaboration, Report No. ATLAS-CONF-2013-014, 2013.
[9] ATLAS Collaboration, Report No. ATLAS-CONF-2013-030, 2013.
[10] CMS Collaboration, Report No. CMS-PAS-HIG-12-053, 2013.
[11] CMS Collaboration, Report No. CMS-PAS-HIG-13-001, 2013.
[12] CMS Collaboration, Report No. CMS-PAS-HIG-13-002, 2013.
[13] CMS Collaboration, Report No. CMS-PAS-HIG-13-003, 2013.
[14] CMS Collaboration, Report No. CMS-PAS-HIG-13-004, 2013.
[15] CMS Collaboration, Report No. CMS-PAS-HIG-13-009, 2013.
[16] S. Chatrchyan *et al.* (CMS Collaboration), J. High Energy Phys. 05 (2013) 145.
[17] S. Chatrchyan *et al.* (CMS Collaboration), J. High Energy Phys. 06 (2013) 081.
[18] T. Aaltonen *et al.* (CDF and D0 Collaborations), Phys. Rev. D **88**, 052014 (2013).
[19] CMS Collaboration, Report No. CMS-PAS-HIG-13-012, 2013.
[20] CMS Collaboration, Report No. CMS-PAS-HIG-13-015, 2013.
[21] D. Carmi, A. Falkowski, E. Kuflik, and T. Volansky, J. High Energy Phys. 07 (2012) 136.
[22] A. Azatov, R. Contino, and J. Galloway, J. High Energy Phys. 04 (2012) 127.
[23] J. R. Espinosa, C. Grojean, M. Muhlleitner, and M. Trott, J. High Energy Phys. 05 (2012) 097.
[24] M. Klute, R. Lafaye, T. Plehn, M. Rauch, and D. Zerwas, Phys. Rev. Lett. **109**, 101801 (2012).
[25] A. Azatov, S. Chang, N. Craig, and J. Galloway, Phys. Rev. D **86**, 075033 (2012).
[26] I. Low, J. Lykken, and G. Shaughnessy, Phys. Rev. D **86**, 093012 (2012).
[27] T. Corbett, O. J. P. Eboli, J. Gonzalez-Fraile, and M. C. Gonzalez-Garcia, Phys. Rev. D **86**, 075013 (2012).
[28] P. P. Giardino, K. Kannike, M. Raidal, and A. Strumia, Phys. Lett. B **718**, 469 (2012).
[29] J. Ellis and T. You, J. High Energy Phys. 09 (2012) 123.
[30] M. Montull and F. Riva, J. High Energy Phys. 11 (2012) 018.
[31] J. R. Espinosa, C. Grojean, M. Muhlleitner, and M. Trott, J. High Energy Phys. 12 (2012) 045.
[32] D. Carmi, A. Falkowski, E. Kuflik, T. Volansky, and J. Zupan, J. High Energy Phys. 10 (2012) 196.
[33] S. Banerjee, S. Mukhopadhyay, and B. Mukhopadhyaya, J. High Energy Phys. 10 (2012) 062.
[34] D. Bertolini and M. McCullough, J. High Energy Phys. 12 (2012) 118.
[35] F. Bonnet, T. Ota, M. Rauch, and W. Winter, Phys. Rev. D **86**, 093014 (2012).

[36] T. Plehn and M. Rauch, Europhys. Lett. **100**, 11002 (2012).
[37] D. Elander and M. Piai, Nucl. Phys. **B867**, 779 (2013).
[38] A. Djouadi, Eur. Phys. J. C **73**, 2498 (2013).
[39] B. A. Dobrescu and J. D. Lykken, J. High Energy Phys. 02 (2013) 073.
[40] G. Moreau, Phys. Rev. D **87**, 015027 (2013).
[41] G. Cacciapaglia, A. Deandrea, G. D. La Rochelle, and J.-B. Flament, J. High Energy Phys. 03 (2013) 029.
[42] T. Corbett, O. J. P. Eboli, J. Gonzalez-Fraile, and M. C. Gonzalez-Garcia, Phys. Rev. D **87**, 015022 (2013).
[43] E. Masso and V. Sanz, Phys. Rev. D **87**, 033001 (2013).
[44] A. Azatov and J. Galloway, Int. J. Mod. Phys. A **28**, 1330004 (2013).
[45] G. Belanger, B. Dumont, U. Ellwanger, J. F. Gunion, and S. Kraml, J. High Energy Phys. 02 (2013) 053.
[46] K. Cheung, J. S. Lee, and P.-Y. Tseng, J. High Energy Phys. 05 (2013) 134.
[47] A. Celis, V. Ilisie, and A. Pich, J. High Energy Phys. 07 (2013) 053.
[48] G. Belanger, B. Dumont, U. Ellwanger, J. F. Gunion, and S. Kraml, Phys. Lett. B **723**, 340 (2013).
[49] A. Falkowski, F. Riva, and A. Urbano, arXiv:1303.1812.
[50] J. Cao, P. Wan, J. M. Yang, and J. Zhu, J. High Energy Phys. 08 (2013) 009.
[51] P. P. Giardino, K. Kannike, I. Masina, M. Raidal, and A. Strumia, arXiv:1303.3570.
[52] T. Alanne, S. Di Chiara, and K. Tuominen, arXiv:1303.3615.
[53] J. Ellis and T. You, J. High Energy Phys. 06 (2013) 103.
[54] A. Djouadi and G. Moreau, arXiv:1303.6591.
[55] W.-F. Chang, W.-P. Pan, and F. Xu, Phys. Rev. D **88**, 033004 (2013).
[56] B. Dumont, S. Fichet, and G. von Gersdorff, J. High Energy Phys. 07 (2013) 065.
[57] P. Bechtle, S. Heinemeyer, O. Stål, T. Stefaniak, and G. Weiglein, arXiv:1305.1933.
[58] M. E. Peskin and T. Takeuchi, Phys. Rev. Lett. **65**, 964 (1990).
[59] M. E. Peskin and T. Takeuchi, Phys. Rev. D **46**, 381 (1992).
[60] M. Baak, M. Goebel, J. Haller, A. Hoecker, D. Kennedy, R. Kogler, K. Mönig, M. Schott, and J. Stelzer, Eur. Phys. J. C **72**, 2205 (2012).
[61] F. Boudjema *et al.*, arXiv:1307.5865.
[62] ATLAS Collaboration, Report No. ATLAS-CONF-2012-161, 2012.
[63] ATLAS Collaboration, Report No. ATLAS-CONF-2012-160, 2012.
[64] M. S. Carena, D. Garcia, U. Nierste, and C. E. M. Wagner, Nucl. Phys. **B577**, 88 (2000).
[65] H. Eberl, K. Hidaka, S. Kraml, W. Majerotto, and Y. Yamada, Phys. Rev. D **62**, 055006 (2000).
[66] A. David *et al.* (LHC Higgs Cross Section Working Group), arXiv:1209.0040.
[67] M. Spira, arXiv:hep-ph/9510347.
[68] M. Spira, Nucl. Instrum. Methods Phys. Res., Sect. A **389**, 357 (1997).
[69] A. Djouadi, J. Kalinowski, and M. Spira, Comput. Phys. Commun. **108**, 56 (1998).
[70] D. Choudhury, R. Islam, A. Kundu, and B. Mukhopadhyaya, Phys. Rev. D **88**, 013014 (2013).
[71] H. E. Logan and M.-A. Roy, Phys. Rev. D **82**, 115011 (2010).
[72] A. Falkowski, S. Rychkov, and A. Urbano, J. High Energy Phys. 04 (2012) 073.
[73] D. Zeppenfeld, R. Kinnunen, A. Nikitenko, and E. Richter-Was, Phys. Rev. D **62**, 013009 (2000).
[74] A. Djouadi *et al.*, arXiv:hep-ph/0002258.
[75] M. Duhrssen, S. Heinemeyer, H. Logan, D. Rainwater, G. Weiglein, and D. Zeppenfeld, Phys. Rev. D **70**, 113009 (2004).
[76] W. Altmannshofer, S. Gori, and G. D. Kribs, Phys. Rev. D **86**, 115009 (2012).
[77] S. Chang, S. K. Kang, J.-P. Lee, K. Y. Lee, S. C. Park, and J. Song, J. High Energy Phys. 05 (2013) 075.
[78] C.-Y. Chen and S. Dawson, Phys. Rev. D **87**, 055016 (2013).
[79] B. Grinstein and P. Uttayarat, J. High Energy Phys. 06 (2013) 094.
[80] B. Coleppa, F. Kling, and S. Su, arXiv:1305.0002.
[81] C.-Y. Chen, S. Dawson, and M. Sher, Phys. Rev. D **88**, 015018 (2013).
[82] O. Eberhardt, U. Nierste, and M. Wiebusch, J. High Energy Phys. 07 (2013) 118.
[83] N. Craig, J. Galloway, and S. Thomas, arXiv:1305.2424.
[84] L. Maiani, A. Polosa, and V. Riquer, Phys. Lett. B **724**, 274 (2013).
[85] G. Aad *et al.* (ATLAS Collaboration), J. High Energy Phys. 02 (2013) 095.
[86] B. Dumont, J. F. Gunion, Y. Jiang, and S. Kraml (work in progress).
[87] N. G. Deshpande and E. Ma, Phys. Rev. D **18**, 2574 (1978).
[88] E. Ma, Phys. Rev. D **73**, 077301 (2006).
[89] R. Barbieri, L. J. Hall, and V. S. Rychkov, Phys. Rev. D **74**, 015007 (2006).
[90] L. Lopez Honorez, E. Nezri, J. F. Oliver, and M. H. G. Tytgat, J. Cosmol. Astropart. Phys. 02 (2007) 028.
[91] M. Krawczyk, D. Sokolowska, P. Swaczyna, and B. Swiezewska, J. High Energy Phys. 09 (2013) 055.
[92] B. Swiezewska, Phys. Rev. D **88**, 055027 (2013).
[93] A. Pierce and J. Thaler, J. High Energy Phys. 08 (2007) 026.
[94] E. Lundstrom, M. Gustafsson, and J. Edsjo, Phys. Rev. D **79**, 035013 (2009).
[95] G. Belanger, F. Boudjema, A. Pukhov, and A. Semenov, arXiv:1305.0237.
[96] A. Arhrib, R. Benbrik, and N. Gaur, Phys. Rev. D **85**, 095021 (2012).
[97] M. Gustafsson, S. Rydbeck, L. Lopez-Honorez, and E. Lundstrom, Phys. Rev. D **86**, 075019 (2012).
[98] B. Swiezewska and M. Krawczyk, Phys. Rev. D **88**, 035019 (2013).
[99] A. Goudelis, B. Herrmann, and O. Stål, J. High Energy Phys. 09 (2013) 106.
[100] H. Georgi and M. Machacek, Nucl. Phys. **B262**, 463 (1985).
[101] J. F. Gunion, R. Vega, and J. Wudka, Phys. Rev. D **42**, 1673 (1990).
[102] C. Englert, E. Re, and M. Spannowsky, Phys. Rev. D **87**, 095014 (2013).

[103] G. Abbiendi *et al.* (ALEPH, DELPHI, L3, OPAL and The LEP working group for Higgs Boson Searches Collaborations), Eur. Phys. J. C **73**, 2463 (2013).

[104] S. Chatrchyan *et al.* (CMS Collaboration), J. High Energy Phys. 07 (2012) 143.

[105] CMS Collaboration, Report No. CMS-PAS-HIG-12-005, 2012.

[106] S. Schael *et al.* (ALEPH, DELPHI, L3, OPAL and LEP Working Group for Higgs Boson Searches Collaborations), Eur. Phys. J. C **47**, 547 (2006).